Applied Catalysis B: Environmental 227 (2018) 240–251

Contents lists available at ScienceDirect

Applied Catalysis B: Environmental

journal homepage: www.elsevier.com/locate/apcatb

Investigating the effect of Fe as a poison for catalytic HDO over sulfided NiMo alumina catalysts

Prakhar Arora[a], Houman Ojagh[a], Jungwon Woo[a], Eva Lind Grennfelt[b], Louise Olsson[a], Derek Creaser[a,*]

[a] Competence Centre for Catalysis, Chemical Engineering, Chalmers University of Technology, SE-412 96, Gothenburg, Sweden
[b] Preem, Gothenburg, Sweden

ARTICLE INFO

Keywords:
Fatty acids
Hydrodeoxygenation
HDO
NiMo
MoS_2
Deactivation
Characterization

ABSTRACT

The effect of iron (Fe) as poison present in renewable feeds was studied during hydrodeoxygenation (HDO) over molybdenum based sulfided catalysts. The study was carried out at 6 MPa and 325 °C in batch reaction conditions. Different concentrations of Fe in the feed were tested over MoS_2/Al_2O_3 and $NiMoS/Al_2O_3$. A notable drop in activity for the conversion of oxygenates was observed for both catalyst systems with an increased concentration of Fe in the feed. However, the changes in selectivity of products was opposite for unpromoted and Ni-promoted catalysts. In the case of the NiMoS catalyst, at higher Fe concentration, the decarbonated product (C_{17} hydrocarbons) decreased while the direct hydrodeoxygenation product (C_{18} hydrocarbons) increased. On the contrary, for the base catalyst (MoS_2), there was a decrease in the yield of direct hydrodeoxygenation (C_{18} hydrocarbons) products and an increase in yield of decarbonated products (C_{17} hydrocarbons). These sulfided catalysts have different sites for these two different reaction routes and they interacted differently with Fe during the deactivation process. With surface deposition of Fe, the ability of these catalysts to create active sites i.e. via sulfur vacancies deteriorated. TEM-EDX results suggested that the effect of Ni as a promoter for the decarbonation route was nullified and a resultant FeMo phase explains the drop in activity and change in selectivity.

1. Introduction

The world's total energy consumption due to the transportation sector stood at 104 quadrillion Btu in 2012, which has been predicted to steadily climb to 155 quadrillion Btu by 2040 [1]. From different sources, liquid fuels like: Petroleum, natural gas-to-liquids, biofuels, and coal-to-liquids; are the preeminent fuel for the fleet of vehicles anywhere in the world. Liquid transportation fuels accounted for a share of 96% of total energy use by the transportation sector in 2012 which is expected to decline only modestly to 88% in 2040 [1].

To meet this huge demand, and in the face of ever rising CO_2 levels and fewer new discoveries of conventional oil, there is a dire need to develop alternate sources of oil for transportation fuels. A new type of renewable liquid fuel, hydroprocessed esters and fatty acids (HEFA) are gaining considerable attention. They are molecularly identical to the fuels derived from fossil resources. These are hydrocarbons produced by hydrotreating feeds like slaughterhouse wastes, vegetable or animal waste oils and forestry residues like tall oil. HEFA biofuels are the most common biofuels produced with a capacity of more than a billion gallons in 2014 [1]. NEXBTL™, Ecofining™, Vegan™ & Hydroflex are some of the commercial processes to produce renewable HEFA fuels in refineries including Neste, ENI, Total & Preem across the world [2–9]. These processes have advantages such as feed flexibility and reduced CO_2 emissions. Also, existing refineries could be modified with minimal investment to produce HEFA biofuels. However, the core of these processes is catalytic hydrodeoxygenation (HDO), which is the removal of oxygen from bio-feeds over a catalyst in the presence of hydrogen to produce predominately water as a side product [10].

In most of the above commercial processes, bi-metallic catalysts such as sulfided CoMo & NiMo are employed during the HDO of oils from bio-origins. Triglycerides, methyl esters and fatty acids are examples of the major components of oils from bioresources, irrespective of their sources. Their chemistry is quite similar because of the carboxyl group they have in common. Also, the fatty acids are in the feedstocks or are the intermediates during the conversion of all of these starting components to hydrocarbons [11]. In this study, we have employed oleic acid (OA) as the realistic model compound since it is the major component of renewable feedstocks like oil from Jatropha (42%), microalgal oil (23%) and tall oil (15%) [12–14] etc. There is a wide range of literature available on the conversion of carboxylic acids and its

* Corresponding author.
E-mail address: derek.creaser@chalmers.se (D. Creaser).

https://doi.org/10.1016/j.apcatb.2018.01.027
Received 24 October 2017; Received in revised form 10 January 2018; Accepted 13 January 2018
Available online 20 January 2018

related feeds using such hydrotreating catalysts [4,14–19]. There was then notable early work by the Murzin group that screened a broad range of catalysts in which it was determined that Pd over C was most active for deoxygenation of stearic acid [20]. Researchers are also working on other catalyst systems like noble metals (Pt, Pd, Ru and Rh) supported on a gamut of interesting supports like ZrO_2, TiO_2, etc [21,22] or in the form of metal-nitrides [23] and phosphides [24] which have yielded promising results. However, their use has so far been limited to laboratory scale evaluations due to factors like cost, availability and poisoning due to for example low quantities of sulfur present in oils from bio-origins. Since the mechanisms for HDS (hydrodesulfurization) and HDO are quite similar, MoS_2 based catalysts are inherently effective for removing oxygen to give hydrocarbons. Such, catalysts become deactivated due to the effect of water, coking and poisoning. Also, these catalyst systems are well-studied as they have been used in refining for fossil feeds for many years now [25]. Still, it is critical to study their deactivation in HDO processes due to the differences in reaction routes, the large amount of water produced as a side-product and the different impurities present in feeds of bio-origin. There are excellent reviews on deactivation of hydrotreating catalysts [26] and hydrodeoxygenation processes [10,27] which cover certain aspects of the aforementioned issues. There are several studies covering different aspects of deoxygenation of esters and fatty acids and related model compounds on promoted Mo based catalysts. Kinetics and the reaction mechanism for HDO of compounds with carboxyl groups has also been studied [4,11,28–30]. The role of promoters like Ni and Co has been studied in detail which gives further insights into the mechanisms and their influence on selectivities [31,32]. And, there are a few articles giving insight into the effect of water [33–35]. Moreover, the effect of different sulfiding agents [36] or partial pressure of H_2S [34,37,38] has been studied in depth. Since the metal-sulfide is the active phase of such catalyst systems, the loss of sulfidity is also a probable cause of deactivation. However, there is only a limited number of contributions studying the effect of impurities during upgrading of oils from bio-origins via catalytic HDO.

Alkali metals like Na, Ca, Mg and non-metals like Phosphorus and Chlorine are present in oils from waste streams and may cause deactivation of the catalyst [35,39]. Kubicka and Horáček concluded that there were synergistic effects between phospholipids and alkali metals causing deactivation of the catalyst, while DMDS (dimethyl disulfide) restrained this deactivation [39]. Also, in a similar study, a close relationship between the amount of sulfiding agent used and the activity of NiMo catalysts was established [40]. Mortensen et al. studied the catalyst stability toward H_2S, H_2O, potassium and organically bound chlorine. However, for a different catalyst system (Ni-MoS_2/ZrO_2) and a feed of phenol and 1-octanol, they observed that poisoning was due to blockage of vacant sites by K along the MoS_2 edges. In two patent studies it was suggested that Fe or its compounds present in renewable feedstocks may play a role in deactivation [41,42]. These renewable feedstocks have high total acid number (TAN) values and are corrosive. As a result, during storage and transportation in iron vessels, acids and their derivative compounds can react to yield Fe containing complexes [27]. However, there are to our knowledge no studies available in the scientific literature that have studied the iron poisoning over Ni/Mo containing catalysts during hydrodeoxygenation, which is the objective of the current work.

We have looked into the poisoning effect of Fe on a NiMoS catalyst during HDO of OA in a batch-reactor setup. Four different iron-oleate complex concentrations in the feed were investigated, in addition to a baseline experiment. We have used higher concentration of Fe in feed to emulate the effect of large quantities of feed treated in a refinery-scale reactor during continuous operations for several months. To build on the initial insights, another set of experiments were carried out, keeping the process conditions the same but with the unpromoted MoS_2 catalyst. During these HDO experiments, it was observed that both catalyst systems deactivated as a function of the poison concentration in the feed. While there was an apparent change in selectivity for products, it was opposite for the Ni-promoted and unpromoted catalyst. Therefore, catalysts (NiMoS) recovered after the HDO experiments were extensively characterized using elemental analysis for carbon and sulfur, Brunauer-Emmett-Teller (BET), Inductively coupled plasma sector field mass spectrometry (ICP-SFMS), Temperature-programmed reduction (TPR) and Transmission electron microscopy (TEM), to elucidate the mechanistic causes of the deactivation and changes in selectivity that could be attributed to Fe.

2. Experimental

2.1. Materials

The γ-Al_2O_3 (PURALOX®, Sasol GmbH) in size range 150–200 μm with a specific surface area of 199 m^2/g, and a pore volume of 0.48 ml/g was employed as support for NiMo and unpromoted Mo catalysts. These two sets of catalysts were prepared by conventional impregnation of the alumina powder using aqueous solutions of $(NH_4)_6Mo_7O_{24}{\cdot}4H_2O$ (Sigma Aldrich) and $Ni(NO_3)_2{\cdot}6H_2O$ (Sigma Aldrich). Initially, 15 wt% Mo was impregnated from a solution of Mo precursor in water on alumina and then dried to remove water. An aliquot was removed at this stage and used as unpromoted catalyst after being calcined. Calcination was done by heating to 450 °C (ramp rate of 10 °C/min) in air for 2 h. The Ni-precursor equivalent to 5 wt% was dissolved in water and impregnated on the dry Mo-based catalysts. Again, the excess water was removed by overnight drying. Finally, the catalyst sample was calcined at 450 °C for 2 h. The detailed procedure can be found here [40]. The catalysts were marked as Mo/Al_2O_3 and NiMo/Al_2O_3.

Oleic acid (Fluka, 90%) was employed as a feedstock in all experiments and used as received. Based on GC analysis, this technical grade oleic acid consisted of the two isomers of oleic acid (86%). The rest was 9-Hexadecenoic acid (palmitoleic acid) about 5%, hexadecanoic acid (palmitic acid) about 4%, tetradecanoic acid (myristic acid) about 3%, while stearic acid and eicosenoic acid were less than 1%. We shall classify these acids other than oleic acid as “Other acid impurities”.

The iron oleate complex which was employed as poison (containing Fe) in the experiments was synthesized following a procedure as described elsewhere [43].

2.2. Catalytic activity measurements

All catalytic reactions in this study were performed in a 300 ml batch reactor (Parr Instruments) equipped with an internal stirrer and an arrangement to collect liquid samples during the experiment. In each of the experiments, 1 g of catalyst and oleic acid (15 wt%) solution in dodecane (Sigma Aldrich), with a total volume of 150 ml were charged. Experiments for both catalysts with different concentrations of iron oleate (poison) were carried out as depicted in Table 1. Both catalysts: Mo/Al_2O_3 and NiMo/Al_2O_3 were sulfided using DMDS (Sigma Aldrich) before each of the experiments following a procedure reported earlier [44]. Dodecane was used as solvent to minimize possible temperature excursions due to reaction exotherms during HDO. 0.1 ml of DMDS was

Table 1
Concentrations of poison in weight ppm studied for each catalyst and experiment abbreviations.

Poison in feed (ppmw)	Catalyst	
	NiMo/Al_2O_3	Mo/Al_2O_3
0	NiMo_0 Fe	Mo_0 Fe
20	NiMo_20 Fe	–
100	NiMo_100 Fe	Mo_100 Fe
500	NiMo_500 Fe	Mo_500 Fe
2000	NiMo_2000 Fe	–

added to the reaction mixture to maintain the catalyst in its sulfided state. All experiments were carried out at 6 MPa, 325 °C and with a stirring rate of 1000 rpm for 330 min. The temperature control was in the range of ± 5 °C. As reported in literature, for similar experimental conditions, this stirring speed was sufficient to rule out limitations of external mass transfer [45]. At the maximum observed initial reaction rate of oleic acid, the Weisz-Prater modulus was estimated to equal 0.05, which indicates that internal mass transfer limitations were also negligible. Details are given in the supporting information. Only the liquid phase products are discussed in this study. After the reaction the catalyst particles were filtered with 200 ml of warm ethanol and dried for subsequent characterization.

Baseline experiments (with no poison) for both catalyst systems were conducted two times with a relative standard deviation of 4% for hydrodeoxygenation conversion activity to ensure repeatability of the setup and protocol. The mole balance based on the feed oleic acid was for every experiment within the range of 90–110% unless otherwise mentioned. The iron content of the synthesized iron-oleate (poison) was determined by ICP. The prepared iron oleate was employed by adding it to the starting reaction mixture. In Table 1, the poison concentration as Fe ppmw, is milligrams of iron per weight (kg) of total liquid feed to the reactor. Experiments are denoted by: (catalyst used)_ (concentration of poison) e.g. "NiMo_X Fe" where X is the concentration of iron in ppmw with respect to the total feed.

2.3. Product analysis

The components of the liquid samples collected during HDO experiments were identified and quantified using GC–MS with a flame ionization detector (FID) (Agilent 7890-5977A). The instrument was configured with a non-polar HP-5 capillary column (L = 30 m, Dia. = 0.25 mm & Film = 0.25 μm). Silylation of samples was executed using BSTFA (N,O-bis(trimethylsilyl) trifluoroacetamide (Sigma Aldrich, ≥99.5%) to increase volatility and enhance the elution of oxygenated compounds in the column. Calibration of the FID was done with external standards for oleic acid, stearic acid, 1-octadecanol, octadecanal, octadecane, heptadecane, hexadecane, pentadecane and tetradecane. Moreover, the peaks from other minor compounds were quantified using the effective carbon number method based on the closest related calibrated compound. Following are the formulas used in this article:

$$\text{Conversion of oxygenates} = \left(1 - \frac{\textit{moles of oxygenates in the sample}}{\textit{moles of starting oxygenates}}\right) \times 100$$

$$\text{Yield\% of } C_{17^+} \text{ \& } C_{18^+} \text{ and min or products} = \frac{\textit{moles of product produced}}{\textit{moles of reactant in feed}} \times 100$$

$$\text{Initial rate of reaction} = \frac{\textit{Initial mmoles of oxygenates} - \textit{mmoles of oxygenates sample @55 mins}}{\textit{time (hr)*wt. ofcatalyst (g)}}$$

$$\text{Rate of formation of } C_{17^+} = \frac{\textit{mmoles of C17+ in 55 mins sample}}{\textit{time (hr)*wt. of catalyst (g)}}$$

$$\text{Rate of formation } C_{18^+} = \frac{\textit{mmoles of C18+ in 55 mins sample}}{\textit{time (hr)*wt. of catalyst (g)}}$$

$$\text{Selectivity of } C_{17^+} = \frac{\textit{mmoles of C17+ at end of reaction}}{\textit{mmoles of C17+ and mmoles of C18+ at end of reaction}}$$

$$\text{Selectivity of } C_{18^+} = \frac{\textit{mmoles of C18+ at end of reaction}}{\textit{mmoles of C17+ and mmoles of C18+ at end of reaction}}$$

2.4. Catalyst characterization

Temperature programmed reaction with hydrogen on spent catalysts was carried out with the catalyst sample in a quartz tube in a temperature controlled furnace. An amount of 50 mg of catalyst was added on the bed in the centre of the quartz tube under a continuous flow of 20 ml/min (at ambient conditions). In the hydrogen temperature programmed reaction (H_2-TPR) experiments with spent catalysts (NiMo_0Fe and NiMo_500Fe), first catalyst samples were degassed in a stream of Ar at 350 °C. Then after cooling to ambient temperature they were exposed to a stream of Ar containing 100 ppm hydrogen for 1 h. Then the concentration of hydrogen was increased to 400 ppm and maintained for 30 min. After that, the temperature was increased to 800 °C with a ramp of 10 °C/min under continuous dosing of hydrogen. The temperature was finally maintained at 800 °C for 30 min. The H_2 and other eluents in the outlet gas stream were monitored with a Hiden Analytical HPR 20 quadrupole mass spectrometer (MS).

To determine the C and H content of spent catalysts, analysis was carried out on a CE Instruments elemental analyzer model EA1110 while for S, analysis was carried out on a Fisons elemental analyzer model NA2000. Both instruments are based on high temperature combustion followed by GC separation and detection by Thermal conductivity.

Crystal phases of the catalyst samples were determined by X-ray diffraction (XRD) using a Bruker AXSD8 Advance X-ray powder diffractometer with CuKα radiation (λ = 1.542A°) at room temperature with scanning parameters of 2θ from 5 to 80° in the scan mode (0.03°, 1 s).

HAADF-STEM imaging of NiMo catalysts samples after being exposed to poison under the reaction conditions were analyzed by a FEI Titan TEM, operating at 300 kV, equipped with EDX. The specimens were prepared by making a suspended solution in ethanol and then letting it dry on the carbon coated copper grid at room temperature. The obtained images were analyzed by ImageJ software for measuring the length of slab and stacking degree of MoS_2. A total of 200 particles were measured for each sample with a relative standard deviation less than 1%. TEM-EDX mapping was done at four different spots for sufficiently long periods in order to stabilize the signal collection.

The amount of metals (Ni, Mo and Fe) in catalyst samples and in the reaction mixture was determined by ICP-SFMS analysis with a Thermo Element XR instrument.

For pore structure analysis, N_2 physisorption was carried out at −196 °C on a Micromeritics ASAP 2010 instrument. Catalyst samples (~30 mg) were degassed at 225 °C under vacuum conditions for 3 h. Specific BET surface area (SBET) was calculated from the adsorption data in the relative pressure range of 0.05–0.2. The pore size distribution curves were calculated using the Barrett-Joyner-Halenda (BJH) method based on analysis of the desorption branch of the isotherm.

3. Results and discussion

This section of the article begins by providing a brief background about hydrodemetallisation of crude feedstocks and reaction pathways in HDO of oleic acid based on existing knowledge. This is followed by a presentation and discussion of the experimental and catalyst characterization results. Initially, the NiMo on alumina catalyst was tested with different poison concentration, but the peculiar change in selectivity with the introduction of poison was intriguing. The effect of the poison on the base catalyst i.e. Mo on alumina, was then investigated to elucidate the interaction of the poison with the active metals.

Removal of metals from heavy feedstocks like residuals and VGO has been of considerable importance in refinery operations. This was due to the relatively poorer quality of oil from discoveries following the "easy oil" phase [46]. Typically, Nickel and Vanadium are the two most common metals present in higher amounts in crude oil. These metals

exist in the form of complexes with porphyrin rings as ligands, also called petroporphyrins [47]. Such metal containing molecules are considered to be catalyst poisons that tend to block the active sites. The ligand molecule and its respective structure geometry controls the coke formation phenomenon. Thus, during hydroprocessing of heavy streams, catalyst deactivation is prevented or delayed by employing a guard bed. Such solutions have been developed over a long time and after many studies on this subject which have provided insights into the mechanisms of deactivation due to metal deposition. To handle the metal poisons present in crude feedstocks, the catalyst pore structures have been tuned to maximize accessibility while trapping the metal deposits. Thus, it is critical to investigate poisons present in renewable feedstocks and their effect on HDO processes. Also, we found similarities regarding loss in activity and location of metal poisons in our study which will be discussed furtheron in Section 3.3.

Catalytic HDO of waste biostreams rich in carboxylic acids and derivatives is gaining a lot of momentum in academia and industry lately as the process can produce hydrocarbons in the jet and diesel fuel range. Triglycerides, fatty acid esters and carboxylic acids (like fatty acids) are the most common model compounds to investigate different aspects of deoxygenation chemistry. In HDO studies with triglyceride as feed, the first step is that of β-elimination in an H_2 atmosphere to give fatty acids as intermediates. Glycerol is a side product which is eventually converted to propane [48]. While fatty acid ester model compounds consist of two types: fatty acid methyl esters (FAMEs) and fatty acid ethyl esters (FAEEs). As per several research studies, ethyl esters proceed via β-elimination while methyl esters via hydrolysis during HDO to produce respective molecules containing a carboxyl functional group. It has been revealed that the Lewis acid sites of alumina facilitate the hydrolysis of methyl esters like methyl heptanoate [19]. There have been a few reports of direct deoxygenation conversion of such molecules without fatty acid included as an intermediate [49]. But we will limit our discussions to HDO of fatty acids and specifically oleic acid since, as discussed above, for many feedstocks a fatty acid molecule is a common intermediate.

Removal of oxygen from oleic acid over the catalyst surface happens in three ways during HDO:

a) A so called direct-HDO in which oxygen is removed as a water molecule
b) Decarbonylation (DCO) in which oxygen is removed as carbon mono-oxide (CO)
c) Decarboxylation (DCO_2) in which oxygen is removed as carbon di-oxide (CO_2).

In the latter two routes; a C_{n-1} hydrocarbon, free from oxygen, is produced while the former produces a C_n alkane or alkene. For simplicity, we will use the term decarbonation (DCO_x) to refer collectively to decarbonylation and decarboxylation. It is important to note that the hydrodeoxygenation or "HDO" is a broader term to define removal of oxygen while "direct-HDO" is specifically used when oxygenated products are converted to produce water as the side product [11,36]. A typical reaction network for HDO of oleic acid over Mo-based catalysts is given in Fig. 1.

As depicted, the first step is a rapid hydrogenation of the double bond in the long hydrophobic part of oleic acid to give stearic acid. Saturation of double bonds occurs relatively quickly since the activation energies are so low such that these reactions are viable even at 100–180 °C over various catalysts [50]. The acid group is then further reduced to 1-octadecanal. As per different reports [4,11,28], such oxygenates containing an aldehyde functional group is the common intermediate for both the possible routes of decarbonylation and direct hydrodeoxygenation. In the direct-HDO route, this intermediate with a carbonyl (−C═O) group could also exist in its enol form due to tautomerism, which was validated by Donnis et al. by employing different ketones with and without α-hydrogen [4]. Then enol would be saturated to give 1-octadecanol. Fatty alcohols are further deoxygenated to give unsaturated isomers of C_{18} hydrocarbons and water as a side product. While, alkenes are eventually reduced to octadecane hydrocarbons. On the other hand, for the DCO_x route, oxygen is removed in tandem with a loss of carbon to yield C_{17} unsaturated products from either stearic acid or octadecanal. These are further reduced to give heptadecane ($C_{17}H_{36}$) as final product.

3.1. HDO of oleic acid over $NiMo/Al_2O_3$

Oleic acid transformation took place at 6 MPa of total pressure and 325 °C in the presence of hydrogen over sulfided NiMo catalysts. A small amount (0.1 ml) of DMDS was added to maintain the sulfidity of the catalysts during the HDO experiments. DMDS decomposition starts at much lower temperatures (150 °C) to give CH_4 and H_2S via methanethiol [51]. GC analysis of liquid samples did not exhibit any peak corresponding to methanethiol as it would be in gas phase due to its very low boiling point. Three groups of products were observed during these experiments irrespective of the Fe poison concentration employed: with two oxygen atoms – Stearic acid and its respective esters; with one oxygen atom – octadecanal and octadecanol; with no oxygen atoms – heptadecane, octadecane and their respective unsaturated isomers and finally compounds corresponding to "other impurities" like palmitoleic acid, palmitic acid and myristic acid (C_{13-16}). The GC–MS analysis also indicated the presence of heavier compounds like stearyl stearate which could be formed by esterification of stearic acid and the intermediate octadecanol. However, the yields of intermediates containing ester groups were found to be much less than 1%. Also, in early samples from these experiments, a very small peak of octadecan-thiol was observed which became undetectable in later samples. Since these experiments were carried out in a batch reactor and the contact times are much longer compared to continuous flow reactors, this is expected in the presence of NiMo catalysts which have high HDS activity as well. During the oleic acid conversion, stearic acid and octadecanol followed similar trends as that of intermediates, where their concentrations pass through a maxima. Liquid samples were collected at progressive time intervals of – 15, 35, 55, 95, 155, 215, 275 and 330 min More samples were collected at the beginning as the change in product distribution was most appreciable early in the experiment. To estimate the selectivity of products from the two main routes – DCO_x and direct HDO; all oxygen free-molecules with the same number of carbon atoms were summed up and plotted against time. While oxygenate conversion was represented as the sum of oleic acid and stearic acid conversion. The conversion and yield profile for major products including "C_{17}^+" being the sum of heptadecane and isomers of heptadecene and "C_{18}^+" being the sum of octadecane and isomers of octadecene with varying concentration of poison are presented in Fig. 2(A)–(C). Also, to estimate the possible catalytic activity of just the Fe poison, an experiment (Al_2O_3_Fe 500) with iron oleate (500 ppmw) and alumina (1 gm) was performed in which no conversion of oleic acid was detected after 330 min.

Fig. 2A shows that the conversion of oxygenates was complete for all experiments except NiMo_2000 Fe, where 7% oxygenates remained after 330 min. In the experiment NiMo_2000 Fe, with the highest Fe concentration, the mass balances for intermediate samples were poor so only results for the sample collected at the end of the experiment (after 330 min) is shown. This sample was directly collected from the reactor and then analyzed and the mass balance was 97%. Poor mass balances of intermediate samples were seen even in a repeated experiment and could be due to the unusually waxy product becoming trapped in the sampling line due to low conversions. Hence, there is just one data point (green diamond) for the NiMo_Fe 2000 experiment in Fig. 2A. It is evident that the increase in conversion slowed down with increasing amounts of iron oleate added to the reaction mixture. Comparing the baseline experiment (NiMo_0 Fe) and NiMo_500 Fe, there were almost no oxygenates remaining just after 95 min while with 500 ppmw of Fe poison it took more than three times the duration to completely

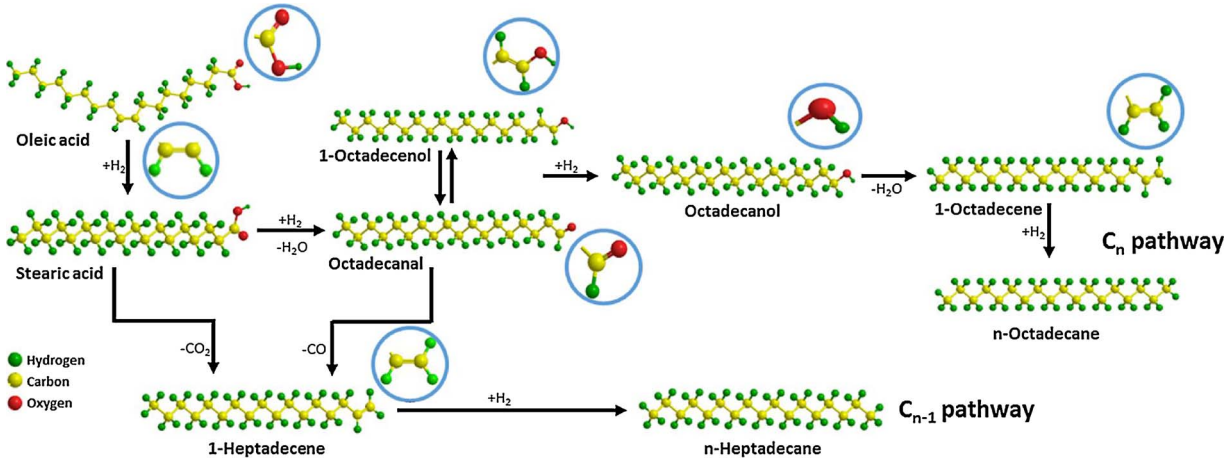

Fig. 1. Reaction scheme for hydrodeoxygenation of oleic acid (OA).

consume the oxygenates. This clearly shows that Fe is poisoning the catalyst by blocking the active sites. Also, Fig. 3A gives the same picture from comparison of the initial activity of the catalysts for oxygenate conversion. There was a steady drop in initial activity of the NiMoS catalyst with increasing poison concentration. It should be noted that the contribution of the oleate ion from the poison is insignificant compared to the amount of OA in the reaction mixture. For the NiMo_500 Fe experiment, the amount of oleate from the poison is only 1.7% of the OA present in the reaction mixture. This extra OA from poison is within the range of measurement accuracy of the addition of OA to the reaction mixture. As depicted in Fig. 1, HDO of oleic acid occurs via two pathways- removal of CO or CO_2 to give heptadecene which is saturated to heptadecane or an initial hydrogenation step to yield aldehyde which is reduced to octadecanol. Then the hydroxyl group is protonated to produce water and unsaturated C_{18} which eventually yields octadecane by hydrogenation. From these two reaction pathways, the preferred route is influenced by the catalyst, reaction conditions, contact time and hydrogen availability which depends on whether a continuous or batch mode of reactor operation is used [11,15,48,52]. For instance, Coumans and Hensen concluded that with a higher concentration of H_2S the decarbonation route is preferred over direct HDO as C_{17} was formed in higher amounts while at lower H_2S concentrations C_{18} selectivity increased. This behavior could be explained either on the basis of competitive adsorption between H_2S and H_2, where the former hindered the latter, or due to the fact that at higher H_2S levels more active sulfided sites like NiS or NiMoS are formed which may promote decarbonation over direct-HDO [11]. From inspection of Figs. 2B and C and 3B it is apparent that the poison has a notable impact on the selectivity. In the experiment with no poison, heptadecane and its isomers form the majority of products while selectivity for direct-HDO products is less. This is in accordance with other studies which have also concluded that decarbonation is the preferred route for such reaction conditions [11,48,52]. Now, as the concentration of poison was increased in the feed, a salient shift in the selectivity from C_{17}^+ to C_{18}^+ products can be observed. Fig. 3B shows that at the end of the NiMo_0 Fe experiment, selectivity for heptadecane and its isomers was 0.76 and it dropped to 0.57 for NiMo_500 Fe experiment. While, the selectivity for products from the direct HDO route increased from 0.24 to 0.43 between baseline to the experiment with higher Fe (500 ppmw). This trend was extended for the highest Fe (2000 ppm) poison experiment, where there was a complete reversal in selectivities for C_{17}^+ and C_{18}^+ products, at 0.16 and 0.84 for C_{17}^+ and C_{18}^+ products respectively. From Fig. 3A, it is apparent that this shift in selectivity is a result of the poison only causing a minor decrease in the rate of formation of direct-HDO products, whereas the decrease in formation of DCO_x products was more severe. In a refinery scale hydrodeoxygenation of such renewable feeds containing fatty acids and triglycerides, the process should aim for a high degree of deoxygenation while retaining as much carbon atoms in the final products as possible. The hydrogen consumption depends on if the oxygen is removed as CO, CO_2 or H_2O. There is a discrete trade off where the decarbonation route yields a lower value product with lower hydrogen consumption assuming the subsequent methanation of CO_x molecules can be avoided. On the other hand, for the direct HDO route no carbon atoms are lost but more hydrogen is needed [4]. The changes in selectivities for products due to poisons present in the feed would apparently result in variation of the hydrogen consumption of a refinery unit.

In Fig. 4, the distribution of different products at 50 and 100% oxygenate conversion are compared for the NiMo_0 Fe (baseline) and NiMo_500 Fe experiments. Here, the values from experimental data were interpolated to estimate the amounts of respective components at 50% conversion. For the poison free experiment, 50% oxygenate conversion was achieved after about 24 mins, whereas with the NiMo_500 Fe experiment, this same level of conversion was achieved after

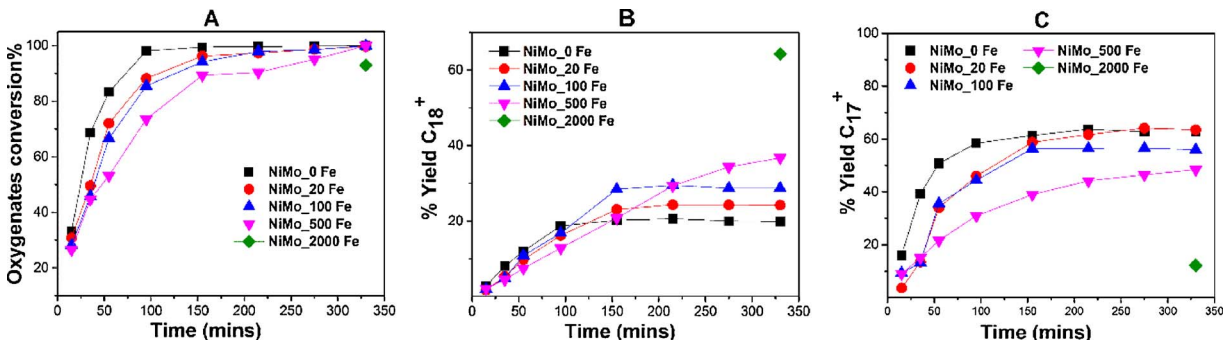

Fig. 2. A, B and C: Oxygenate conversion and selectivity for major products during HDO of Oleic acid over NiMoS/γ-Al_2O_3 with varying concentrations of poison (Fe-oleate).

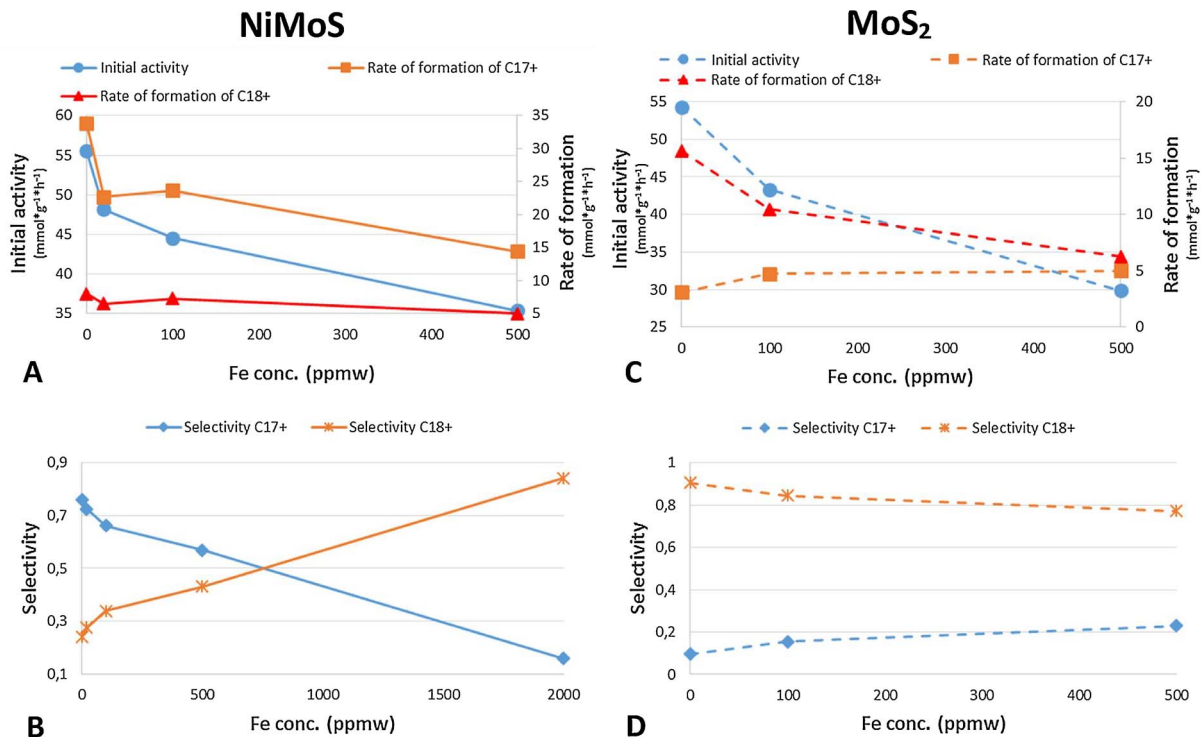

Fig. 3. A B, C and D: Comparison of initial activity and rate of formation for C_{17} & C_{18} and final selectivities (after 330 mins) for DCOx & HDO routes for different poison (Fe-oleate) concentrations with NiMoS (solid line) and MoS_2 (dash line).

50 mins. For both experiments, 100% oxygenate conversion was achieved within the complete experiment run of 330 mins. It shows that the amount of hydrocarbons from other acid impurities were comparable both at 50% and 100% conversion for both the NiMo_500 Fe and baseline experiments. At 100% conversion they converged to ca. 12% of the total products. This is in agreement with the total amount of other acids present in oleic acid based on GC analysis. There was minimal cracking activity with the NiMoS catalyst at these reaction conditions and regardless of the Fe poison loading. These results are in accordance with the study by Boyas et al., where they observed 3.2 wt% of cracked products at a slightly higher temperature of 350 °C with the same catalyst system [48]. In a comparative study of HDO of esters, it has been reported that Ni based catalysts more selectively produce saturated hydrocarbons compared to CoMo catalysts which are more selective for unsaturated hydrocarbons [19]. We observed a trend such that upon increasing the Fe poison concentration, the alkene/alkane ratio for all the samples increased for both C_{17} and C_{18} products even at the same conversion. This indicates that the Fe poison inhibits the hydrogenation

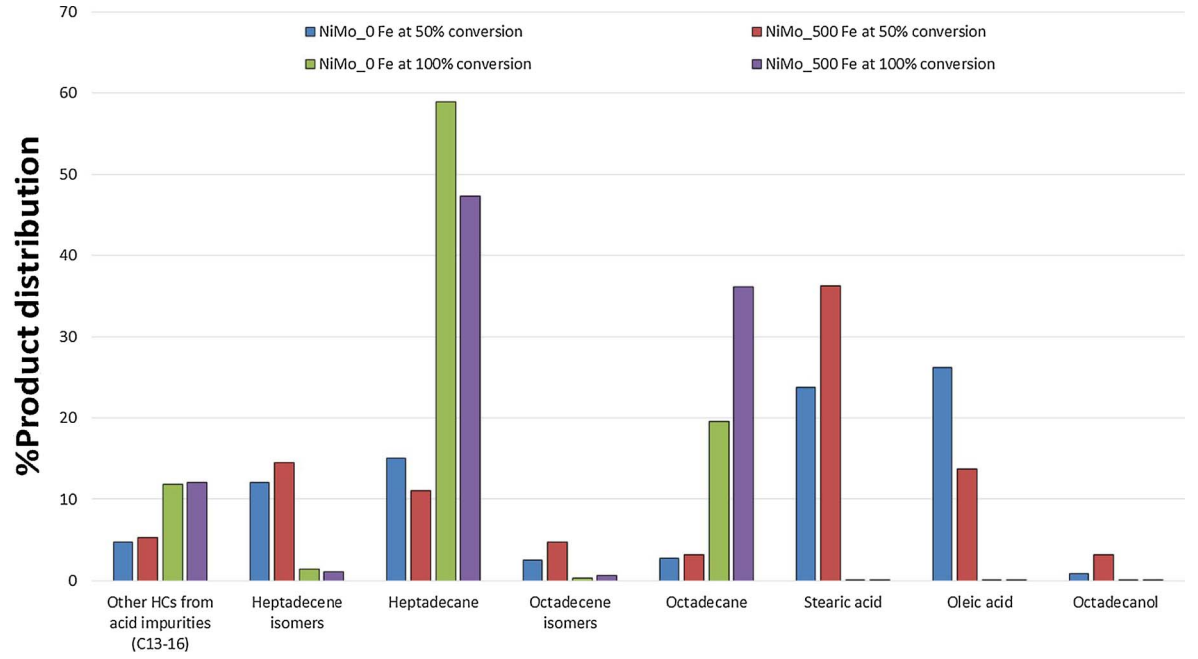

Fig. 4. Product distributions for NiMo catalyst with no poison (NiMo_ 0 Fe) and high poison (NiMo_500 Fe) at 50 and 100% oxygenate conversion respectively. Results at 50% conversion interpolated from experiments.

reactions just like it does the conversion of oxygenates. Also, it has been suggested that the saturation of alkenes is delayed until the conversion of carboxyl containing compounds is complete, as they bind more strongly to the active sites [11,28]. In this study, we see a coupled effect of these two phenomenon; Fe hindering the subsequent hydrogenation and causing lower activity so that OA and SA were bound to the catalyst surface for much longer. The Fe poison evidently slows down most all of the reaction steps shown in Fig. 1 and as a result, higher concentrations of intermediate species could be detected and their appearance was delayed. This is validated by experimental results, since total concentration of oxygenates for NiMo_ 0 Fe and NiMo_500 Fe were very close at 67 and 71% after 15 mins while the ratio of alkene/alkane for both C17 and C18 was greater in the case of the high poison experiment. From Fig. 4, at 50% oxygenate conversion, SA is 12% higher for the poisoned experiment. It is evident that the Fe poison causes a different distribution of the remaining oxygenates at 50% conversion. With Fe there is more SA remaining rather than OA. This indicates that the Fe has a lesser impact on slowing the hydrogenation of OA to SA, but a relatively greater impact on the further conversion of SA. This further validates that Fe poison leads to a decrease in activity by blocking of active sites for this catalyst system. Similarly, other oxygenates like octadecanal and octadecanol were present more in experiments with higher poison concentration. Octadecanal was not observed at all in the baseline experiment while for the NiMo_500 Fe experiment, it appeared after between 35 and 55 mins. Octadecanol was at 3.2% for the 500 ppm Fe experiment while less than 1% for Fe free experiment. This also explains the change in the selectivity pattern of higher octadecane with higher Fe poison employed.

3.2. HDO of oleic acid over Mo/Al_2O_3

In the second part of the study, unpromoted molybdenum sulfide catalysts were tested in the same batch setup and at the same reaction conditions (6 MPa and 325 °C) as above. Three experiments were carried out with different poison concentrations (Table 1). Results for the oxygenate conversions and yields of C_{17}^+ and C_{18}^+ hydrocarbons for the baseline experiment with no poison, and for an intermediate concentration (100 ppmw Fe) and the highest poison concentration (500 ppmw Fe) are shown in Fig. 5. The major intermediates like stearic acid, octadecanal, octadecanol and stearyl stearate and products like heptadecane and octadecane and their respective unsaturated isomers were observed with the MoS_2 catalyst as well. The two most noticeable differences were generally higher amounts of 1-octadecanol formed at lower and intermediate oxygenate conversions and difference in the selectivity for the DCO_x and direct-HDO routes. Here, with or without the poison, octadecane was formed in majority while heptadecane was the minor product. Since 1-octadecanol is an intermediate of the direct-HDO route, it can be expected to be observed in higher concentrations when the selectivity for the direct-HDO route is higher. In Fig. 3D, we could observe how selectivity is skewed towards octadecane products for all concentrations of Fe employed. These observations that the unpromoted molybdenum catalyst is more selective for direct-HDO is congruent with other studies [31,53,54]. From Fig. 5(A–C) for the baseline experiment (Mo_0 Fe), oxygenate conversion was close to completion after 95 min while for the highest poison concentration it took three times longer to completely consume oxygenates. Also, Fig. 3C, shows how the initial activity steadily dropped with the poison concentration. So it is evident that Fe is blocking the active sites of the MoS_2 phase, similar to that of the NiMo catalyst. Though, from comparison of the levels of conversion of oxygenates for unpromoted and Ni promoted molybdenum catalysts at each sampling point, it is clear that the NiMo catalyst is slightly more active. It is also evident from initial activity for oxygenate conversion (Fig. 3A and C), that Ni promoted catalysts have a slightly higher activity compared to the base MoS_2 catalysts at all different poison concentrations tested. In literature, it has been reported that catalyst activity follows the order of $NiMo/Al_2O_3$ > Mo/Al_2O_3 > Ni/Al_2O_3 for similar reactions over a range of temperature [17].

At 500 ppm of Fe, there is a drop in activity of 36% and 44% for NiMoS and MoS_2 respectively. The promoting effect of Ni for deoxygenation is considered to be due to a lowering of the energy level for C═O hydrogenation and cleavage of C−O on the NiMoS phase, as has been reported by Raybaud et al. based on DFT calculations combined with experimental results [53]. Also, it has been mechanistically explained due to the fact that at Ni promoted sites the antibonding S-metal d states are below the Fermi level which is due to weakening of bonds of S to the S-edges [55]. When comparing the selectivities, it looks like the MoS_2 active sites have a preference for hydrogenation which enables direct-HDO over decarbonation. From Fig. 3B and D, it is evident that selectivity for the direct-HDO product is over 80% with no poison while that of the decarbonation route is only at 8% which is opposite to that of the NiMo catalysts. This promotion in activity and change in selectivity by adding Ni to Mo containing catalyst could also be explained by the catalytic cycle proposed by Brillouet et al. [28]. Molybdenum based catalysts have sulfur vacancies on the edges of the MoS_2 phase, which are commonly accepted as active sites [56]. This catalytic cycle initiates by heterolytic splitting of a hydrogen molecule which results in a sulfur vacancy. Then, the carbonyl group of the acids are adsorbed on metal centers. The promoters, like Ni or Co, weaken the metal-sulfur bond resulting in more sulfur vacancies and hence higher activity. While the shift in the selectivity towards heptadecane is due to an increase in electron density of sulfur atoms because of Ni. This enables the more basic sulfur anion to eliminate the proton from the β position. This increases the likelihood for the cleavage of the C−C bond and formation of C_{n-1} hydrocarbon. We observe an opposite trend in terms of shift in selectivity as poison concentration is increased, when comparing these two catalysts. On MoS_2, the products from the direct HDO route (octadecane and unsaturated isomers) decreased from 80 to 60% while the decarbonation products (C_{17}^+) increased from 8 to 18%. From Fig. 3D, it can be seen that this results from the Fe poison causing a decrease in the rate of formation of direct-HDO products at the same time as a modest increase in the rate of formation of decarbonation products occurred.

Fig. 6 shows the changes in the product distribution over the

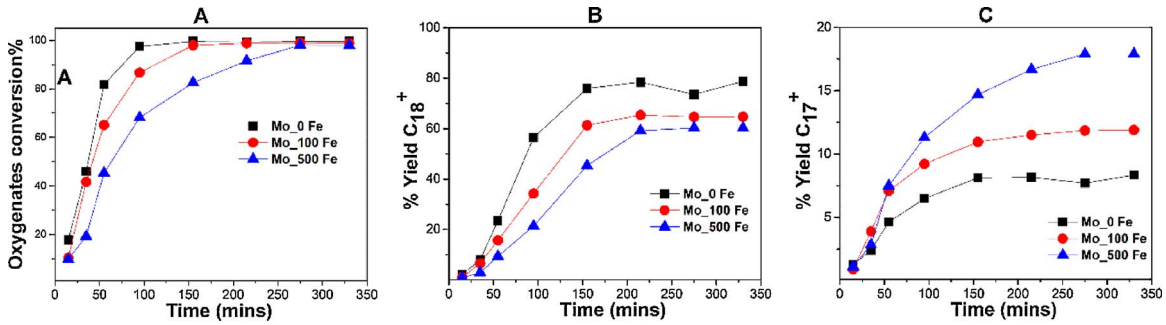

Fig. 5. A, B & C: Selectivity of major products during HDO of Oleic acid over MoS_2/γ-Al_2O_3 with varying concentrations of poison (Fe-oleate).

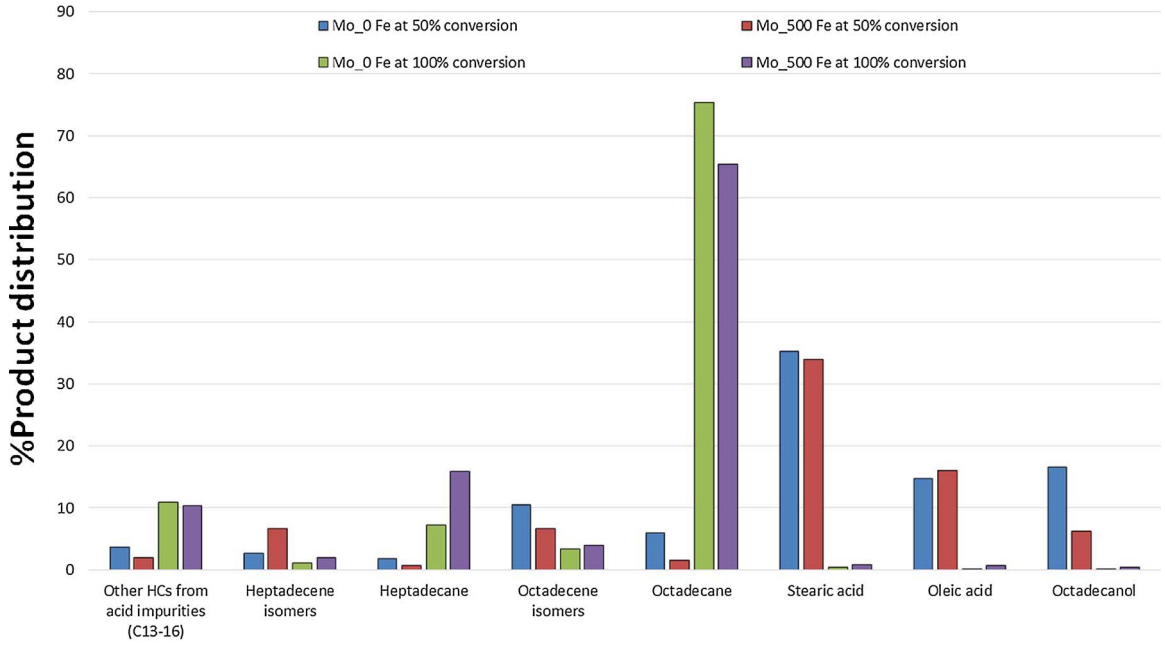

Fig. 6. Product distribution for MoS_2 catalyst with no poison (Mo_ 0 Fe) and high poison (Mo_500 Fe) at 50 and 100% oxygenate conversion respectively. Results at 50% conversion interpolated from experiments.

Molybdenum catalyst with and without Fe poison at 50% oxygenate conversion and at end of the reaction by when 100% conversion was achieved. Here, the values from experimental data were interpolated to estimate the amounts of respective components at 50% conversion. Here, the baseline (Mo_0 Fe) experiment is compared with the highest poison (Mo_Fe 500) concentration. The trend for the shorter hydrocarbons ($C_{13–16}$), produced from other acids present in the feed, is similar to that seen for the Ni promoted molybdenum catalyst. Also, the negative impact of the Fe poison on the hydrogenation activity of catalysts was seen here as well as the increased alkene/alkane ratio. After 50% conversion of oxygenates, for the baseline experiment the alkene/alkane ratio for C_{17} was 1.5 and for C_{18} it was 1.8 while for the Mo_500 Fe experiment these ratios were several times higher at 10.4 (for C_{17}) and 4.4 (for C_{18}). It should be noted that even the first step of conversion of oleic to stearic acid is slower for MoS_2 compared to NiMo and this is further slowed due to poisoning. If we compare the total amount of oleic acid, stearic acid and octadecanol for NiMo_500Fe and Mo_500Fe, after one hour it is 54 and 67% respectively. In the base experiments, NiMo_0 Fe and Mo 0 Fe, total oxygenates are 18% and 47% respectively. This clearly exhibits that the Fe poison has more impact on the NiMo catalyst though in absolute terms the molybdenum catalyst has lost almost two-third of its activity. While the impact of Fe on the changes in selectivity is greater for the NiMo catalysts. In the case of the NiMo catalyst, the decrease in selectivity for C_{17} products was 20% while for the MoS_2 catalyst the decrease in selectivity for C_{18} products was only 12% when the Fe-oleate concentration was increased from zero to 500 ppm. The decrease in the yield of the HDO route intermediate 1-octadecanol caused by Fe for the MoS_2 catalyst was expected due to the reduced selectivity for the direct-HDO route.

3.3. Catalyst deactivation and characterization

Textural and compositional properties of the catalyst samples are listed in Table 2. Comparison of the surface area of the NiMo_0 Fe and NiMo_500 Fe catalyst samples can indicate the extent of pore blockage by iron. It has been reported in a patent that in commercial scale production of hydrotreated vegetable oils etc. at refineries, there have been issues related to unpredictable pressure drop causing unplanned shutdowns [42]. The surface area of the catalyst can be blocked due to coke formation from unwanted side reactions and irreversibly adsorbed species during the course of reaction. Here, in the baseline experiment, a drop of 7% was observed in the surface area. There was a decrease in surface area and pore volume by 16 and 23% respectively following the 330 min HDO experiment for the NiMoS catalyst due to the Fe poison. Over time, with continuous pore plugging this should accelerate deactivation and eventually increase pressure drop over a catalyst bed. Also, these molybdenum based catalysts are known to be most active in sulfide phase. So the elemental contents of sulfur and carbon of the catalysts recovered after the 330 min HDO experiments were analyzed (Table 2). There is not much variation in the carbon content for all the samples as it ranged between 0.76–1.3 wt% except for the NiMo_2000Fe sample where it was relatively higher at 3.52 wt%. This could be due to the incomplete conversion of oxygenates for this experiment, where c.a. 7% remained unconverted after 330 min. The molecules containing oxygen are likely to bind irreversibly to the catalyst surface and they contribute to the higher carbon content in this particular sample. If this experiment had been continued for a longer duration to reach complete conversion of oxygenates, it is likely that the carbon content would have been lower also for these conditions. These carbon depositions are comparable to other studies. Senol

Table 2
Textural properties and elemental content of sulfur and carbon on fresh and recovered catalyst samples.

	BET surface area [m^2g^{-1}]	Pore Volume [cm^3g^{-1}]	Average Pore Size [Å]	S [wt%]	C [wt%]
γ-Al_2O_3	199	0.48	97.6	< 0.1	0.1
NiMo (fresh)	141.5	0.31	87.6	< 0.1	0.04
Mo (fresh)	154.5	0.33	88.2	< 0.1	0.04
NiMo_0 Fe[a]	131.3	0.29	86.6	8.3	0.9
NiMo_20 Fe[a]	–	–	–	6.9	0.76
NiMo_100 Fe[a]	–	–	–	7.7	1.17
NiMo_500 Fe[a]	118.9	0.24	80.8	7.6	0.72
NiMo_2000 Fe[a]	–	–	–	10.9	3.52
Mo_0 Fe[a]	144.7	0.31	87.1	6.0	1.1
Mo_100 Fe[a]	–	–	–	5.8	1.3
Mo_500 Fe[a]	132.3	0.26	81.7	5.8	1.6

[a] after 330 min of HDO reaction.

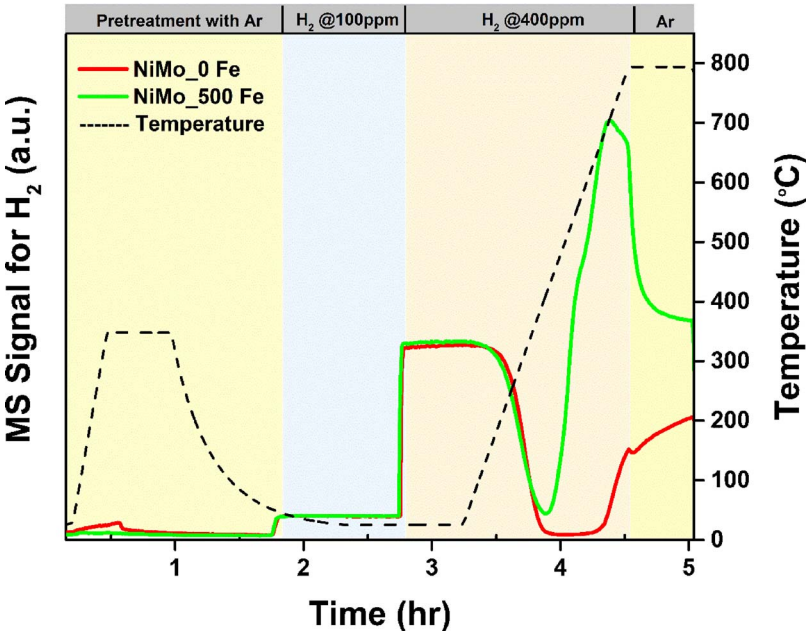

Fig. 7. Pretreatment and H_2 temperature programmed reaction on recovered catalyst samples NiMo_0 Fe and NiMo_500 Fe.

reported a coke deposit of 2.7 wt% on a NiMo catalyst after 1 h of batch reaction with n-heptanoic acid while it was 2–3 wt% with n-tetradecane as solvent in a study done by Irina et al. [19,52]. Assuming the species Ni_3S_2 and MoS_2 are formed on the catalysts, the sulfur saturated Ni promoted and unpromoted molybdenum catalysts would have 7.2 and 6.1 wt% respectively sulfur contents. From the results in Table 2, the sulfur content is in the range 6–11% and it is evident that there has not been any significant loss of sulfur or the sulfided phase as such. The slightly higher amounts of reported sulfur than the expected saturated levels could be due to loosely bound sulfur species on the sulfided form of catalyst [35]. In addition to this, there could be some uptake of sulfur by Fe as well to give FeS like compounds.

The H_2-TPR results are shown in Fig. 7. For both catalyst samples negligible adsorption of H_2 was detected at ambient temperature. Adsorption of H_2 only started at about 270 °C for both catalysts. The poison exposed sample desorbed the same amount of hydrogen at temperatures slightly above 400 °C as it adsorbed at lower temperatures. Interestingly, it was observed that hydrogen on the spent catalyst with no poison was more reactive since from about 150 °C through to 800 °C many S containing molecules like H_2S were released. This indicates that the amount of labile sulfur is higher in the absence of the Fe poison. This is required for the creation of sulfur vacancies which is considered to be the first step in the catalytic cycle of transition metal sulfides and thus related to the catalytic activity of the catalyst for both HDO and DCO_x routes [28]. Since Fe salts are moderate oxidants it is possible that the sulfide phase has been oxidized and rendered inert for the temperature programmed reaction with hydrogen [42].

Table 3 shows the ICP analysis results for the Ni, Mo and Fe contents of the freshly synthesized catalyst, as well as for samples recovered after the HDO experiment from the liquid phase after 330 min of reaction and that of the recovered liquid phase/hydrocarbon. Directly after synthesis, the unpromoted catalyst contained 9.2 wt% Mo, whereas the Ni promoted catalyst contained 3.3 wt% Ni and 9.3 wt% Mo. The atomic ratio of Ni/Ni + Mo was constant at 0.37, for all of the experiments with varying poison concentration, which suggests that there was no leaching from the catalyst and thus no possibility for homogenous reactions. It should be noted that for all Mo based catalysts no Fe was detected in the liquid phase after reaction which suggests that essentially all of the Fe poison became deposited on the catalysts. Only for the experiment with the inactive alumina support (Alumina_500 Fe) was Fe found to remain in the liquid phase with essentially none

Table 3
ICP analysis results of fresh and recovered catalysts and liquid phase following reaction.

	Atomic ratio		Liquid Phase
	Ni/Ni + Mo	Fe/Fe + Ni + Mo	Fe (mg/kg)
NiMo (fresh)	0.36	< 0.01	–
Mo (fresh)	–	< 0.01	–
NiMo_0 Fe	0.37	0.01	< 0.2
NiMo_20 Fe	0.36	0.05	< 0.2
NiMo_100 Fe	0.36	0.07	< 0.2
NiMo_500 Fe	0.37	0.28	< 0.2
NiMo_2000 Fe	0.37	0.57	< 0.2
Mo_0 Fe	–	0.01	< 0.2
Mo_100 Fe	–	0.09	< 0.2
Mo_500 Fe	–	0.36	< 0.2
Alumina_500 Fe	–	–	15.1

deposited on the support. This suggests that most of the Fe probably becomes deposited on or near the metal centers of these supported catalyst systems. This also shows that Fe deposition is closely linked to catalytic activity, since Fe deposition was minimal for the inert alumina support. As a result, a probable mechanism for the deposition of Fe is the deoxygenation of the oleate ligands of the Fe-oleate complex which results in Fe being deposited at or near active sites. This is similar to the general understanding of hydrotreating of crude w.r.t. hydrodemetallisation (HDM), where the metals like V and Ni from hydrogenolysis are deposited at active sites as well [57].

TEM was employed to investigate the morphological structure and dispersion of the active phase, namely MoS_2 slabs. In addition, TEM-EDX mapping was performed in order to study the distribution of Fe with respect to Ni and Mo on the spent catalysts. Fig. 8 shows the HR-TEM image of the NiMo_500 Fe sample, recovered after the 330 mins of HDO experiment. HAADF-STEM images of NiMo_500Fe sample recovered after the HDO experiment and their EDX mapping images are displayed in Fig. 9. EDX mapping done at other spots is available in the supporting information (Fig. S2a & S2b) for reference. In Fig. 8, the edge planes of the MoS_2 slabs are clearly seen which are oriented in line with or at a small angle from the electron beam. It seems that these homogenously distributed MoS_2 structures tend to bend with increasing length. This suggests greater evidence of interaction between the MoS_2 structures and the alumina support. Also, at a few spots in the HR-TEM image (Fig. 8), several slabs are cross-linked over each other. The

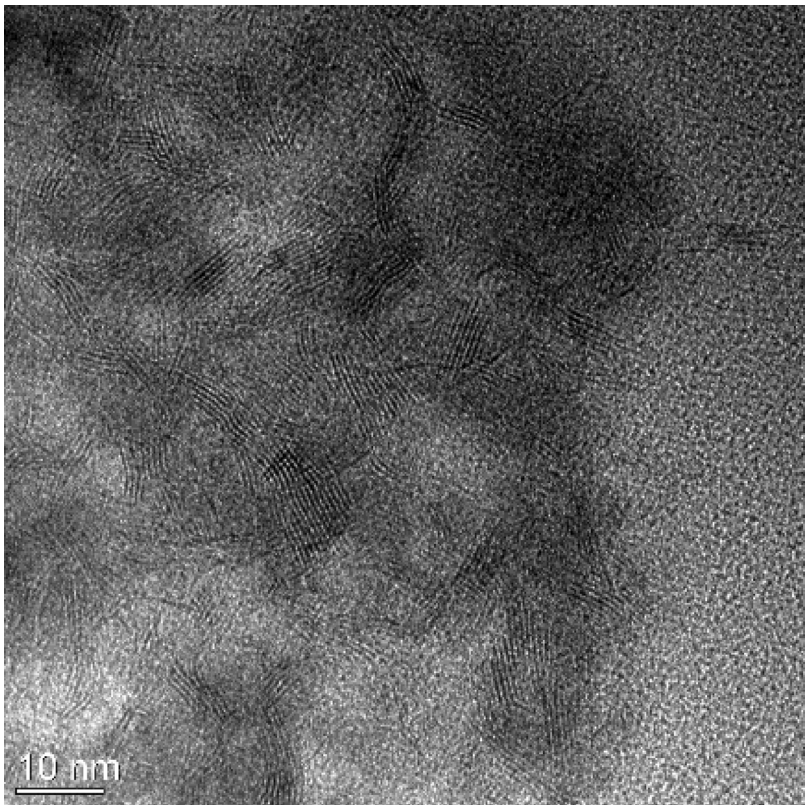

Fig. 8. HR-TEM image of catalyst recovered after 330 mins of HDO (NiMo_500 Fe) experiment.

distribution of slab lengths and stacking degree of MoS_2 were calculated to gain insights about the effect of Fe on the active phase. Table 4 displays the stacking degree and the average length of slabs for catalysts (NiMo_0 Fe and NiMo_500 Fe) recovered after the HDO experiment. As it could be clearly seen both the stacking degree and average slab length of MoS_2 increased by 41% and 50% respectively when Fe was added to the experiment. It is known that there is a direct correlation between higher dispersion corresponding to lower stacking of the MoS_2 slabs and activity for the hydrogenation of olefins on these transition metal sulfides [58]. It is well accepted that such transition metal sulfides (CoMoS or NiMoS) exist in two types of phases with Ni or Co present on the monocrystalline phase of MoS_2. Type I phase is relatively less sulfided with a low stacking degree, and stronger interaction with the alumina support via Mo-O-Al bridges. While the type II phase is fully sulfided and highly stacked, which is due to a weaker interaction with alumina

Table 4
Distribution of stacking degrees and average lengths of MoS_2 slabs from measurements in the HR-TEM images of catalysts after NiMo_0 Fe and NiMo_500 Fe experiments.

	NiMo_0 Fe	NiMo_500 Fe
Stacking degree	2.2	3.1
Avg length (nm)	3.4	5.1

[59]. Fe like Co and Ni belongs to the same group (VIII), and it is probable that their higher loadings on the MoS_2 phase can result in less interaction with alumina. This competing interaction of MoS_2 between support and other metals may explain the observed higher stacking with greater Fe deposition. Also, there was a noticeable difference in the attainable sharpness of the resolution of the slab structures, where the slabs of the NiMo_500 Fe appeared more blurry with less distinct

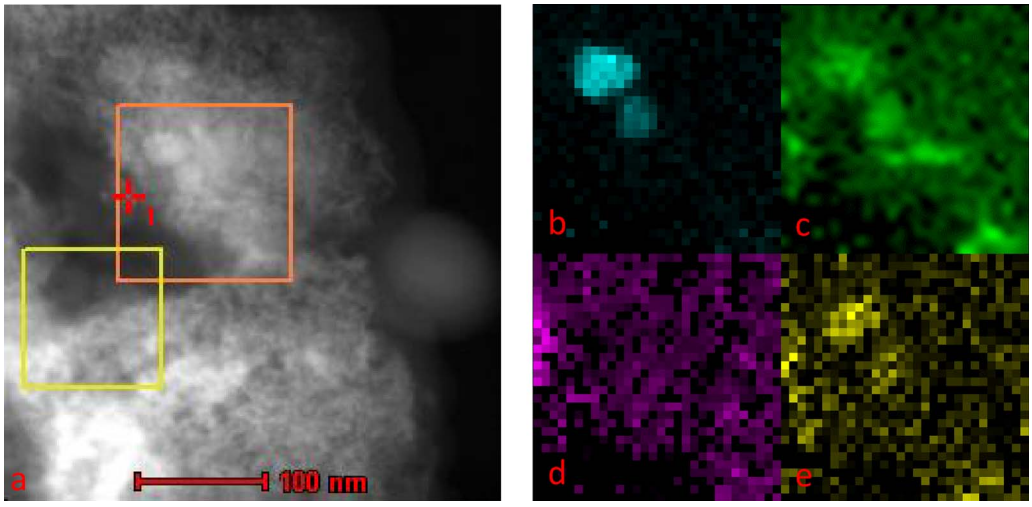

Fig. 9. (a) HAADF-STEM image NiMoS2 recovered after 330 mins of HDO (NiMo_500 Fe) experiment and corresponding EDX mapping according to elements: (b) nickel (c) iron (d) molybdenum and (e) sulfur.

boundary lines [60]. Also, the HR-TEM image from NiMo_0 Fe experiment can be found in supporting information (Fig. S1) for comparison. This could occur due to oxidation since Fe is known to be a moderate oxidizing agent [35,52]. It may indicate the Fe poisons promote oxidation and prevent the resulfidation of the active phase. This hypothesis is congruent with the results shown in Fig. 7 for H_2-TPR where it was found that the spent catalyst unexposed to Fe formed H_2S to a much greater degree than the catalyst poisoned by Fe.

When Ni or Co is used as promotor on the base MoS_2 catalysts, these metals decorate the edges of these slabs [59]. Then there are vacancies present on the edge sites which are considered to be responsible for the activity of the catalysts [56]. Since these edge sites are more exposed, Fe could preferentially deposit at these positions. A DFT study has reported that potassium (K) doping on MoS_2 could bind to the edges of the MoS_2 slabs which reduced the CO dissociation [61]. The locations where K adsorbs on the MoS_2 slabs has been further validated by experiments involving poisoning due to potassium on $NiMoS_2/ZrO_2$ catalysts [35]. EDX elemental maps in Fig. 9 provide a picture of the relative distributions of the active phase and poison. In Fig. 9, the area within the orange square was scanned for a prolonged period to obtain the distribution of Fe, Ni, Mo and S as depicted in the images to the right. It is interesting to note how the distribution of Fe is overlapping with the signals from Ni, although Fe is also observed in other areas as well. In the EDX spectrum, areas richer in the Ni phase also have more bright spots corresponding to Fe distribution. This extends to the fact that the more active Ni promoted active sites would be affected more in comparison to that of the base MoS_2 phase by Fe deposited due to HDO of the oleate ligand. It could also be hypothesized that iron could form a FeMo phase, and thus Fe like Ni may act as a weaker promoter and form sites that promote the DCOx route. It has been concluded in previous studies that Fe could act as a promoter although weaker than Ni during hydrodesulfurization [62]. Thus, it is probable that Fe could act as a weaker promoter for HDO reactions if deposited Fe can partially form a FeMo phase.

In summary, Fe-oleate in the fatty acid feed can play various roles to change the activity and selectivity of NiMo and Mo based catalysts. Firstly, during HDO of the oleate ligand, Fe is preferentially deposited at or near active sites. Fe poisoned sites are less active, simply due to the blockage of sites and/or pores, but also Fe may reduce the dispersion of the active phase and/or hinder sulfur mobility and the formation of sulfur vacancies that act as active sites. For the Ni promoted catalyst, Fe is deposited nearby and thus mainly deactivates Ni promoted sites which shifts the selectivity of this catalyst toward formation of direct-HDO products by mainly reducing the formation rate of DCO_x products (see Fig. 3A). However, for the MoS_2 base catalyst, Fe both deactivates sites and can also forms new sites which like Ni promote the DCOx route and selectivity for C17+ products. This is consistent with the reduced rate of formation of direct-HDO products and simultaneous increase in formation of DCOx products due to Fe (see Fig. 3C).

4. Conclusions

The deactivation of NiMoS and MoS_2 catalysts was studied at different concentrations of Fe poison during HDO of OA. Renewable feeds due to high total acid number (TAN) are known to have corrosion related issues during transportation and storage resulting in formation of iron salts. Iron oleate was employed as a complex of Fe for poison and added to the batch reactor with the feed and solvent. DMDS was added as a sulfur source to maintain the active sulfided phase of these catalysts.

Activity for both unpromoted and promoted catalysts dropped due to increasing the amounts of the Fe poison and it took longer to achieve complete conversion of oxygenates in the presence of Fe, which could be very negative for the process. It is therefore of utmost importance to minimize the deactivation of the catalyst, due to contaminants present in the renewable feeds. Interestingly, there was a change in the selectivities for these two transition metal sulfides in opposite ways. The main products for both catalysts were C_{17} and C_{18} hydrocarbons, with C_{17} products preferred for NiMoS and C_{18} products preferred for MoS_2. For the MoS_2 catalyst, selectivity for the decarbonation route ($C_{17}+$) increased while in case of NiMoS, yield for hydrodeoxygenation ($C_{18}+$) products increased due to Fe-oleate.

Characterization of recovered catalysts after HDO experiments helped to elucidate reasons behind the drop in activity and changes in selectivity. A substantial amount of pores were plugged due to the Fe poison which was evident from BET results. This contributed to lower hydrodeoxygenation activity. Excessive coking due to Fe promoting unwanted side reactions as a cause of pore plugging was ruled out since the carbon content in recovered catalysts was independent of the Fe concentration. A loss of the sulfide phase of the catalyst could have explained the loss in activity. But, the results from elemental analysis of sulfur showed that only a minor drop in sulfur content was observed for all spent catalysts and this was also independent of the Fe addition. However, the results from temperature programmed reaction with hydrogen suggested that the Fe poison negatively impacted the ability to react with hydrogen to produce H_2S or sulfur vacancies. TEM images yielded insights regarding the distribution of Fe and explained how the role of Ni as a promoter of DCOx product formation was subdued. It was concluded that Fe preferentially capped the Ni particles which led to a reduced activity and reduced selectivity for the DCOx route which otherwise is a preferred reaction route with the NiMoS system. This was further validated by the fact that Fe deposition at the most active sites should be favored, since it was found that Fe deposition was directly linked to catalyst activity. While, in the case of MoS_2, the Fe poison both caused deactivation and partially formed the less active FeMo phase which explains the lower overall activity along with the modest increase in DCO_x product formation which shifted the selectivity away from direct-HDO products.

Conflicts of interest

None.

Acknowledgements

This work is performed at the Competence Centre for Catalysis in collaboration with Preem. We would like to acknowledge Formas (Contract: 239-2012-1584 and 239-2014-164) and Preem for the financial support. In addition, we acknowledge the help from Stefanie Tamm and Muhammad Abdus Salam from the Chemical engineering division of Chalmers University of Technology with the GC–MS method development and analysis.

Appendix A. Supplementary data

Supplementary data associated with this article can be found, in the online version, at https://doi.org/10.1016/j.apcatb.2018.01.027.

References

[1] International Energy Outlook 2016; US Department of Energy, DOE/EIA-0484(2016) from May 2016, https://www.eia.gov/outlooks/ieo/pdf/0484(2016).pdf.
[2] W. Vermeiren, G.N. Van, A process for the production of bio-naphtha from complex mixtures of natural occurring fats&oils, Google Patents, 2012.
[3] T.N. Kalnes, K.P. Koers, T. Marker, D.R. Shonnard, A technoeconomic and environmental life cycle comparison of green diesel to biodiesel and syndiesel, Environ. Progress Sustain. Energy 28 (2009) 111–120.
[4] B. Donnis, R.G. Egeberg, P. Blom, K.G. Knudsen, Hydroprocessing of bio-Oils and oxygenates to hydrocarbons. Understanding the reaction routes, Top. Catal. 52 (2009) 229–240.
[5] J.A. Petri, T.L. Marker, Production of diesel fuel from biorenewable feedstocks, Google Patents, 2009.
[6] E. Koivusalmi, J. Myllyoja, J. Matikainen, Process for producing a saturated hydrocarbon component, Google Patents, 2007.

[7] M. Laakkonen, J. Myllyoja, B. Toukoniitty, M. Hujanen, A. Saastamoinen, A. Toivo, Improved process for manufacture of liquid fuel components from renewable sources, Google Patents, 2013.
[8] R.G. Egeberg, K.G. Knudsen, N.J. Blom, J.A. Hansen, Hydroconversion process and catalyst, Google Patents, 2017.
[9] T. Chapus, N. Dupassieux, A. Daudin, Process for the continuous hydrogenation of triglyceride containing raw materials using a nickel and molybdenum-based catalyst, Google Patents, 2015.
[10] E. Furimsky, Catalytic hydrodeoxygenation, Appl. Catal. A: Gen. 199 (2000) 147–190.
[11] A.E. Coumans, E.J.M. Hensen, A model compound (methyl oleate oleic acid, triolein) study of triglycerides hydrodeoxygenation over alumina-supported NiMo sulfide, Appl. Catal. B: Environ. 201 (2017) 290–301.
[12] S.-J. Lee, S. Go, G.-T. Jeong, S.-K. Kim, Oil production from five marine microalgae for the production of biodiesel, Biotechnol. Bioproc. Eng. 16 (2011) 561–566.
[13] A. Kumar, S. Sharma, Potential non-edible oil resources as biodiesel feedstock: an Indian perspective, Renew. Sustain. Energy Rev. 15 (2011) 1791–1800.
[14] J.M. Anthonykutty, K.M. Van Geem, R. De Bruycker, J. Linnekoski, A. Laitinen, J. Räsänen, A. Harlin, J. Lehtonen, Value added hydrocarbons from distilled tall oil via hydrotreating over a commercial NiMo catalyst, Ind. Eng. Chem. Res. 52 (2013) 10114–10125.
[15] G.W. Huber, P. O'Connor, A. Corma, Processing biomass in conventional oil refineries: production of high quality diesel by hydrotreating vegetable oils in heavy vacuum oil mixtures, Appl. Catal. A: Gen. 329 (2007) 120–129.
[16] O.İ. Şenol, T.R. Viljava, A.O.I. Krause, Hydrodeoxygenation of methyl esters on sulphided NiMo/γ-Al2O3 and CoMo/γ-Al2O3 catalysts, Catal. Today 100 (2005) 331–335.
[17] D. Kubička, L. Kaluža, Deoxygenation of vegetable oils over sulfided Ni, Mo and NiMo catalysts, Appl. Catal. A: Gen. 372 (2010) 199–208.
[18] S. Palanisamy, B.S. Gevert, Hydroprocessing of fatty acid methyl ester containing resin acids blended with gas oil, Fuel Process. Technol. 126 (2014) 435–440.
[19] O.İ. Şenol, E.M. Ryymin, T.R. Viljava, A.O.I. Krause, Reactions of methyl heptanoate hydrodeoxygenation on sulphided catalysts, J. Mol. Catal. A: Chem. 268 (2007) 1–8.
[20] M. Snåre, I. Kubičková, P. Mäki-Arvela, K. Eränen, D.Y. Murzin, Heterogeneous catalytic deoxygenation of stearic acid for production of biodiesel, Ind. Eng. Chem. Res. 45 (2006) 5708–5715.
[21] Y. Bie, J. Lehtonen, J. Kanervo, Hydrodeoxygenation (HDO) of methyl palmitate over bifunctional Rh/ZrO2 catalyst: insights into reaction mechanism via kinetic modeling, Appl. Catal. A: Gen. 526 (2016) 183–190.
[22] P.T. Do, M. Chiappero, L.L. Lobban, D.E. Resasco, Catalytic deoxygenation of methyl-octanoate and methyl-stearate on Pt/Al2O3, Catal. Lett. 130 (2009) 9–18.
[23] J. Monnier, H. Sulimma, A. Dalai, G. Caravaggio, Hydrodeoxygenation of oleic acid and canola oil over alumina-supported metal nitrides, Appl. Catal. A: Gen. 382 (2010) 176–180.
[24] Z. Zhang, M. Tang, J. Chen, Effects of P/Ni ratio and Ni content on performance of γ-Al2O3-supported nickel phosphides for deoxygenation of methyl laurate to hydrocarbons, Appl. Surf. Sci. 360 (Part A) (2016) 353–364.
[25] P. Grange, Catalytic hydrodesulfurization, Catal. Rev. 21 (1980) 135–181.
[26] E. Furimsky, F.E. Massoth, Deactivation of hydroprocessing catalysts, Catal. Today 52 (1999) 381–495.
[27] P.M. Mortensen, J.D. Grunwaldt, P.A. Jensen, K.G. Knudsen, A.D. Jensen, A review of catalytic upgrading of bio-oil to engine fuels, Appl. Catal. A: Gen. 407 (2011) 1–19.
[28] S. Brillouet, E. Baltag, S. Brunet, F. Richard, Deoxygenation of decanoic acid and its main intermediates over unpromoted and promoted sulfided catalysts, Appl. Catal. B: Environ. 148–149 (2014) 201–211.
[29] P. Kumar, S.R. Yenumala, S.K. Maity, D. Shee, Kinetics of hydrodeoxygenation of stearic acid using supported nickel catalysts: effects of supports, Appl. Catal. A: Gen. 471 (2014) 28–38.
[30] M. Snåre, I. Kubičková, P. Mäki-Arvela, K. Eränen, J. Wärnå, D.Y. Murzin, Production of diesel fuel from renewable feeds: kinetics of ethyl stearate decarboxylation, Chem. Eng. J. 134 (2007) 29–34.
[31] P. Priecel, D. Kubička, L. Čapek, Z. Bastl, P. Ryšánek, The role of Ni species in the deoxygenation of rapeseed oil over NiMo-alumina catalysts, Appl. Catal. A: Gen. 397 (2011) 127–137.
[32] H. Zhang, H. Lin, Y. Zheng, The role of cobalt and nickel in deoxygenation of vegetable oils, Appl. Catal. B: Environ. 160–161 (2014) 415–422.
[33] O.İ. Şenol, T.R. Viljava, A.O.I. Krause, Hydrodeoxygenation of aliphatic esters on sulphided NiMo/γ-Al2O3 and CoMo/γ-Al2O3 catalyst: the effect of water, Catal. Today 106 (2005) 186–189.
[34] E. Laurent, B. Delmon, Study of the hydrodeoxygenation of carbonyl, carboxylic and guaiacyl groups over sulfided CoMo/γ-Al2O3 and NiMo/γ-Al2O3 catalyst, Appl. Catal. A: Gen. 109 (1994) 97–115.
[35] P.M. Mortensen, D. Gardini, C.D. Damsgaard, J.-D. Grunwaldt, P.A. Jensen, J.B. Wagner, A.D. Jensen, Deactivation of Ni-MoS2 by bio-oil impurities during hydrodeoxygenation of phenol and octanol, Appl. Catal. A: Gen. 523 (2016) 159–170.
[36] O.İ. Şenol, T.R. Viljava, A.O.I. Krause, Effect of sulphiding agents on the hydrodeoxygenation of aliphatic esters on sulphided catalysts, Appl. Catal. A: Gen. 326 (2007) 236–244.
[37] O.İ. Şenol, E.M. Ryymin, T.R. Viljava, A.O.I. Krause, Effect of hydrogen sulphide on the hydrodeoxygenation of aromatic and aliphatic oxygenates on sulphided catalysts, J. Mol. Catal. A: Chem. 277 (2007) 107–112.
[38] E.-M. Ryymin, M.L. Honkela, T.-R. Viljava, A.O.I. Krause, Insight to sulfur species in the hydrodeoxygenation of aliphatic esters over sulfided NiMo/γ-Al2O3 catalyst, Appl. Catal. A: Gen. 358 (2009) 42–48.
[39] D. Kubička, J. Horáček, Deactivation of HDS catalysts in deoxygenation of vegetable oils, Appl. Catal. A: Gen. 394 (2011) 9–17.
[40] H. Ojagh, D. Creaser, S. Tamm, P. Arora, S. Nyström, E. Lind Grennfelt, L. Olsson, Effect of dimethyl disulfide on activity of NiMo based catalysts used in hydrodeoxygenation of oleic acid, Ind. Eng. Chem. Res. 56 (2017) 5547–5557.
[41] P. Knuuttila, J. Nousiainen, A. Rissanen, Process and apparatus for producing hydrocarbons from feedstocks comprising tall oil and terpene-compounds, Google Patents, 2011.
[42] T. Ouni, V. Sippola, P. Lindqvist, Renewable oil with low iron content and its use in hydrotreatment process, Google Patents, 2012.
[43] Y.-J. Lee, K.-W. Jun, H.S. Park, R.C. Chikate, A simple chemical route for the synthesis of γ-Fe2O3 nano-particles dispersed in organic solvents via an iron–hydroxy oleate precursor, J. Ind. Eng. Chem. 14 (2008) 38–44.
[44] Y. Shi, J. Chen, J. Chen, R.A. Macleod, M. Malac, Preparation and evaluation of hydrotreating catalysts based on activated carbon derived from oil sand petroleum coke, Appl. Catal. A: Gen. 441–442 (2012) 99–107.
[45] M. Snåre, I. Kubičková, P. Mäki-Arvela, D. Chichova, K. Eränen, D.Y. Murzin, Catalytic deoxygenation of unsaturated renewable feedstocks for production of diesel fuel hydrocarbons, Fuel 87 (2008) 933–945.
[46] J.M. Oelderik, S.T. Sie, D. Bode, Progress in the catalysis of the upgrading of petroleum residue: a review of 25 years of R&D on Shell's residue hydroconversion technology, Appl. Catal. 47 (1989) 1–24.
[47] P.C.H. Mitchell, Hydrodemetallisation of crude petroleum: fundamental studies, Catal. Today 7 (1990) 439–445.
[48] R. Sotelo-Boyás, Y. Liu, T. Minowa, Renewable diesel production from the hydrotreating of rapeseed oil with Pt/Zeolite and NiMo/Al2O3 catalysts, Ind. Eng. Chem. Res. 50 (2011) 2791–2799.
[49] D. Kubička, P. Šimáček, N. Žilková, Transformation of vegetable oils into hydrocarbons over Mesoporous-Alumina-Supported CoMo catalysts, Top. Catal. 52 (2009) 161–168.
[50] M. Konkol, W. Wróbel, R. Bicki, A. Gołębiowski, The influence of the hydrogen pressure on kinetics of the canola oil hydrogenation on industrial nickel catalyst, Catalysts 6 (2016) 55.
[51] S. Texier, G. Berhault, G. Pérot, V. Harlé, F. Diehl, Activation of alumina-supported hydrotreating catalysts by organosulfides: comparison with H2S and effect of different solvents, J. Catal. 223 (2004) 404–418.
[52] I.V. Deliy, E.N. Vlasova, A.L. Nuzhdin, E.Y. Gerasimov, G.A. Bukhtiyarova, Hydrodeoxygenation of methyl palmitate over sulfided Mo/Al2O3, CoMo/Al2O3 and NiMo/Al2O3 catalysts, RSC Adv. 4 (2014) 2242–2250.
[53] M. Ruinart de Brimont, C. Dupont, A. Daudin, C. Geantet, P. Raybaud, Deoxygenation mechanisms on Ni-promoted MoS2 bulk catalysts: a combined experimental and theoretical study, J. Catal. 286 (2012) 153–164.
[54] I. Simakova, O. Simakova, P. Mäki-Arvela, A. Simakov, M. Estrada, D.Y. Murzin, Deoxygenation of palmitic and stearic acid over supported Pd catalysts: effect of metal dispersion, Appl. Catal. A: Gen. 355 (2009) 100–108.
[55] L.S. Byskov, J.K. Nørskov, B.S. Clausen, H. Topsøe, DFT calculations of unpromoted and promoted MoS2-based hydrodesulfurization catalysts, J. Catal. 187 (1999) 109–122.
[56] J.R. Anderson, M. Boudart, Catalysis, Springer-Verlag, Berlin Heidelberg, 1996.
[57] M.S. Rana, J. Ancheyta, S.K. Maity, P. Rayo, Characteristics of maya crude hydrodemetallization and hydrodesulfurization catalysts, Catal. Today 104 (2005) 86–93.
[58] L. Qu, R. Prins, Hydrogenation of cyclohexene over in situ fluorinated NiMoS catalysts supported on alumina and Silica–Alumina, J. Catal. 207 (2002) 286–295.
[59] H. Topsøe, B.S. Clausen, F.E. Massoth, Hydrotreating catalysis, in: J.R. Anderson, M. Boudart (Eds.), Catalysis: Science and Technology, Springer Berlin Heidelberg, Berlin, Heidelberg, 1996, pp. 1–269.
[60] P.J. Kooyman, J.A. Rob van Veen, The detrimental effect of exposure to air on supported MoS2, Catal. Today 130 (2008) 135–138.
[61] A. Andersen, S.M. Kathmann, M.A. Lilga, K.O. Albrecht, R.T. Hallen, D. Mei, Adsorption of potassium on MoS2(100) surface: a first-principles investigation, J. Phys. Chem. C 115 (2011) 9025–9040.
[62] S. Gobolos, Q. Wu, O. Andre, F. Delannay, B. Delmon, Correlation between hydrodesulphurization activity and reducibility of unsupported MoS2-based catalysts promoted by group VIII metals, J. Chem. Soc. Faraday Trans. Phys. Chem. Condens. Phases 82 (1986) 2423–2434.